The 9th European Congress on Computational Methods in Applied Sciences and Engineering
ECCOMAS Congress 2024
3–7 June 2024, Lisboa, Portugal

OPTIMIZATION OF A SEISMIC METASURFACE BASED ON POWER FLOW FOR REDUCTION OF GROUND VIBRATION DUE TO SURFACE LOADS

Z. KABIRIAN, D. CARNEIRO, G. DEGRANDE AND G. LOMBAERT

KU Leuven, Department of Civil Engineering, Kasteelpark Arenberg 40, B-3001 Leuven, Belgium
e-mail: zohre.kabirian@kuleuven.be

Key words: Seismic metasurfaces, optimization, power flow, vibration reduction

Summary. An optimization method is presented to improve the performance of a seismic metasurface to mitigate environmental ground vibration in a wide frequency range. A 3D coupled finite element – boundary element method is used to solve the dynamic soil-structure interaction problem. We consider the wave field generated by a point load at the soil's surface as a representative case of environmental ground vibration. The metasurface consists of resonators modeled as single-degree-of-freedom systems on top of square concrete foundations that are positioned on a homogeneous halfspace. We compute the power flow through a vertical plane in the soil behind the metasurface as a global performance metric. The integrated power flow over a range of frequencies is minimized to achieve broadband vibration reduction. The soil is Initially, the parameters of each row of resonators are considered as design variables. Subsequently, the parameters of each resonator are optimized individually to investigate the trade-off between performance and complexity of the design. A local optimization method with a gradient-based algorithm is used. Both optimized solutions are compared to a conventional solution with graded resonance frequencies and uniform mass distribution, known as an inverse metawedge. In all cases, the algorithm converges to a solution at the upper limit of the total mass, but with a non-uniform mass distribution across the resonators. Both optimized metasurfaces enhance broadband vibration reduction and achieve a more uniform reduction over a large volume of soil when compared to the inverse metawedge. The performance of both optimized designs is similar, indicating that increased complexity does not significantly improve performance.

1 INTRODUCTION

The expansion of railway networks in urban areas has raised concerns about ground-borne vibration, which can cause discomfort to residents and disrupt sensitive equipment [1]. While various vibration mitigation measures, such as trenches with in-fill materials and heavy surface masses, have been explored [2, 3, 4], reducing low-frequency vibrations remains challenging. Building on advancements in metamaterials in electromagnetics, photonics, and phononics, seismic metamaterials have recently been used as effective solutions for vibration mitigation [5].

Periodic arrangements of non-resonant seismic metamaterials generate Bragg scattering, which prevents wave propagation [6]. Conversely, locally resonant seismic metamaterials do not depend on structural periodicity, allowing for smaller dimensions and spacing than surface

wavelengths. These locally resonant metamaterials have shown the ability to control wave propagation at low frequencies, making them a promising solution for mitigating railway-induced vibrations.

Colombi et al. investigate the impact of forests on the attenuation of Rayleigh waves in soft sedimentary soil at frequencies below 150 Hz [7] and introduce a resonant metawedge metasurface to control seismic Rayleigh waves [8]. This metasurface, made of vertical resonators with graded resonance frequencies, can convert Rayleigh waves into shear waves or reflect them, creating a seismic rainbow effect. A study on optimizing local adaptive resonators in a mass-in-mass structure demonstrates that spatially varying unit-cell properties enhance seismic protection effectiveness [9]. A recent study of metasurfaces on layered soils shows a significant drop in performance when the resonators are not excited by body waves traveling in the upper layer [10]. Further study on how the performance of seismic metasurfaces can be improved is required.

This paper explores the potential of optimization for enhancing the performance of seismic locally resonant metasurfaces in the reduction of environmental ground vibration in a broad frequency band and a large volume of soil. In order to measure the transmitted vibration, the power flow through a vertical plane in the soil behind the metasurface is calculated. The integrated power flow over a wide frequency range is minimized in the optimization problem. Forward modeling relies on a 3D coupled finite element-boundary element method (FE-BE), where the metasurface is modeled as single-degree-of-freedom systems on top of square concrete foundations interacting with layered soil. The mass and resonance frequency of the resonators are the design variables.

The paper is organized as follows. In section 2, the formulation of the optimization problem is described. It states how power flow analysis is used to quantify the vibration mitigation performance of the metasurface. Section 3 describes the properties of the considered cases. In section 4, the obtained optimized metasurfaces on a homogeneous soil are described and results are compared to the inverse metawedge. Conclusions are given in section 5.

2 Formulation of the optimization problem

Figure 1 shows an array of N_x by N_y resonators positioned with lattice constants a_x and a_y on top of a horizontally layered soil represented by the unbounded domain $\Omega_{\mathrm{s}}^{\mathrm{e}}$. The metasurface is placed at a distance D from the origin of the coordinate system where the source S is located. The metasurface serves to shield a large volume of soil from the generated wave field. A 3D coupled finite element-boundary element method is used to solve the soil-structure interaction problem [10].

The aim of the optimization is to tune the parameters of the resonators so that the vibration reduction performance of the metasurface is maximized. The problem is formulated as follows:

$$\boldsymbol{\theta}^* = \arg\min_{\boldsymbol{\theta}} \{g(\boldsymbol{\theta})\} \tag{1}$$

$$\begin{aligned} &\text{s.t. } h(\boldsymbol{\theta}) \leq 0 \\ &\theta_{\mathrm{l}} < \theta_i \leq \theta_{\mathrm{u}} \end{aligned} \tag{2}$$

where $\boldsymbol{\theta}$ is the vector of design variables, $g(\boldsymbol{\theta})$ is the objective function which measures the performance of the metasurface and $h(\boldsymbol{\theta})$ is the vector of inequality constraints. Additional constraints defining the lower and upper bounds θ_{l} and θ_{u} of the design variables are added.

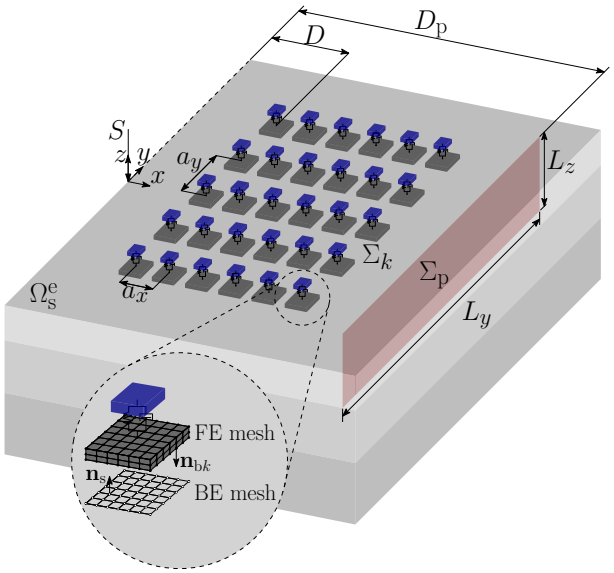

Figure 1: An array of surface resonators on a layered soil.

In order to capture the global performance of the metasurface in terms of transmitted wave energy, we consider the mean power flow through a plane Σ_p in the soil located on the transmission path behind the metasurface (figure 1). This metric enables us to quantify the effectiveness of the metasurface in vibration reduction in a global way without focusing on the response of local receivers. Therefore the objective function in the optimization problem is the integrated power flow through a plane Σ_p in a frequency range between ω_l and ω_u as:

$$g(\boldsymbol{\theta}) = \int_{\omega_\mathrm{l}}^{\omega_\mathrm{u}} \langle \hat{P}(\Sigma_\mathrm{p}, \omega, \boldsymbol{\theta}) \rangle \, \mathrm{d}\omega \tag{3}$$

A hat on a variable denotes its representation in the frequency domain. The basic principles of power flow analysis [11] are briefly recapitulated. Consider an infinitesimal boundary $\mathrm{d}\Gamma$ with unit outward normal vector $\mathbf{n}$ through a point Q of a continuum Ω (figure 2). The instantaneous power flow $p^\mathbf{n}(t)$ through $\mathrm{d}\Gamma$ at time t, or the rate of work performed by the tractions $\mathbf{t}^\mathbf{n}(t)$, is defined as the inner product of the traction vector $\mathbf{t}^\mathbf{n}(t)$ and the velocity vector $\mathbf{v}(t)$:

$$p^\mathbf{n} = -\mathbf{t}^\mathrm{n} \cdot \mathbf{v}, \tag{4}$$

where the minus sign ensures a positive transmission of energy per unit of time through the surface $\mathrm{d}\Gamma$ from the inner to the outer side as shown in figure 2 [12].

Using Cauchy's stress formula, the instantaneous power flow can be written as follows:

$$p^\mathbf{n} = -(\boldsymbol{\sigma} \cdot \mathbf{n}) \cdot \mathbf{v} = -(\boldsymbol{\sigma}^\mathrm{T} \cdot \mathbf{v}) \cdot \mathbf{n} = \mathbf{p} \cdot \mathbf{n}, \tag{5}$$

where $\mathbf{p}(t)$ is the instantaneous power flow density vector [11]. The mean power flow density vector $\langle \hat{\mathbf{p}}(\omega) \rangle$ is the time average of $\mathbf{p}(t)$ over a period of vibration $2\pi/\omega$ and can be obtained as [13]:

$$\langle \hat{\mathbf{p}} \rangle = -\frac{1}{2} \mathrm{Re}\big(\hat{\boldsymbol{\sigma}}^* \cdot \hat{\mathbf{v}}\big) = -\frac{1}{2} \mathrm{Re}\big(\mathrm{i}\omega \, \hat{\boldsymbol{\sigma}}^* \cdot \hat{\mathbf{u}}\big), \tag{6}$$

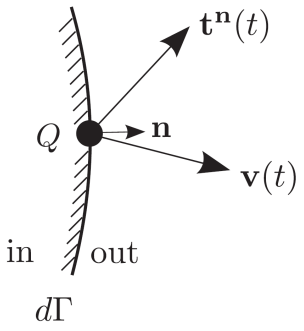

Figure 2: Traction vector $\mathbf{t}^{\mathrm{n}}(t)$ and velocity vector $\mathbf{v}^{\mathrm{n}}(t)$ in a point Q on an infinitesimal boundary $\mathrm{d}\Gamma$ of a continuum Ω with outward unit normal vector $\mathbf{n}$.

where $*$ denotes the complex conjugate. The total mean power flow (briefly referred to as the power follow in the following) $\langle \hat{P}(\Gamma, \omega) \rangle$ through a surface Γ is calculated as follows:

$$\langle \hat{P} \rangle = \int_{\Gamma} \langle p^{\hat{\mathbf{n}}} \rangle \, \mathrm{d}\Gamma = \int_{\Gamma} \langle \hat{\mathbf{p}} \rangle \cdot \mathbf{n} \, \mathrm{d}\Gamma. \tag{7}$$

To compute the power flow $\langle \hat{P}(\Sigma_{\mathrm{p}}, \omega, \boldsymbol{\theta}) \rangle$ through Σ_{p} the velocities and the tractions are computed with the boundary element method [10].

A nonlinear gradient-based optimization algorithm based on sequential quadratic programming as implemented in the Matlab function fmincon has been adopted to solve the optimization problem. For this method, the sensitivities of the objective function and constraints are required at each iteration. The gradients are computed with the adjoint method which is efficient when the number of a design variables is high.

3 Case description

An array of 100 resonators ($N_x = 10$ by $N_y = 10$) with lattice constants $a_x = a_y = 2\,\mathrm{m}$ is considered on top of a homogeneous soil with a shear wave velocity $C_{\mathrm{s}} = 150\,\mathrm{m/s}$, dilatational wave velocity $C_{\mathrm{p}} = 300\,\mathrm{m/s}$ and density $\rho = 1800\,\mathrm{m/kg}^3$. The hysteretic material damping ratios in shear and volumetric deformation are $\beta_{\mathrm{s}} = 0.02$ and $\beta_{\mathrm{p}} = 0.02$, respectively. The first row of the resonators is located at a distance $D = 12\,\mathrm{m}$ from the source. Each resonator is modeled as a single-degree-of-freedom system connected to the center of a rigid square concrete foundation of dimensions $0.5\,\mathrm{m} \times 0.5\,\mathrm{m} \times 0.1\,\mathrm{m}$ and mass 62.5 kg. Rigid body kinematics are assumed for the foundation, and hence, no FE model is used. A unit point load is applied on the surface of the soil in the frequency range between $\omega_{\mathrm{l}} = 2\pi \times 30\,\mathrm{rad/s}$ and $\omega_{\mathrm{u}} = 2\pi \times 70\,\mathrm{rad/s}$ to represent a broadband source.

The power flow in equation (3 serves as the objective function for the optimization problem and is calculated through a plane with dimensions $L_y = 22$ m and $L_z = 4$ m. Two cases are considered in the optimization problem to investigate the trade-off between complexity and performance. In case 1, all resonators located on a same row have the same mass and resonance frequency. In the literature, this configuration is known as a metawedge configuration [14]. Therefore, the mass and resonance frequency of each row ($i = 1, 2, ..., \mathrm{N}_x$) of the resonators are optimized, leading to 20 design variables θ. In case 2, the mass and resonance frequency

(with fixed base) of each resonator k ($k = 1, 2, ..., \mathrm{N}_x\mathrm{N}_y$) are optimized, resulting in 200 design variables θ.

The mass of the resonators is bounded in a range between $\theta_\mathrm{l} = 1\,\mathrm{kg}$ and $\theta_\mathrm{u} = 300\,\mathrm{kg}$. A lower bound $\theta_\mathrm{l} = 10\,\mathrm{Hz}$ and an upper bound $\theta_\mathrm{u} = 150\,\mathrm{Hz}$ are imposed for the resonance frequency. To maximize the performance of the metasurface for a given cost, the total mass of the resonators is limited to 20000 kg. The modal damping ratio of the resonators is chosen as $\xi = 0.03$.

In the following section, the performance of the optimized metasurface is compared with an inverse metawedge [10].

4 Vibration mitigation performance of the optimized metasurface

An inverse metawedge consisting of resonators with fixed base resonance frequency increasing from 30 Hz to 70 Hz in the $x-$direction is considered as a reference solution (figure 3a). Each resonator has a mass of 200 kg. After 110 iterations the optimization converges to the case 1 configuration as shown in figure 3b. As expected, the algorithm converges to the maximum allowable mass. The general trend is that the mass of the resonators increases from 140 kg on the first row to 300 kg on the third row and then decreases to 60 kg on the last row. The resonance frequency of the resonators is between 40 Hz and 70 Hz. The resonance frequency starts at 65 Hz for the first row, decreases to 40 Hz for the third row, and follows a similar pattern for the next three rows. The last four rows have higher resonance frequencies between 65 Hz and 70 Hz. Figure 3c shows the optimized configuration for case 2. The algorithm after 320 iterations converges to a symmetric configuration with respect to the $y-$axis as expected because of the problem symmetry. The mass is mostly distributed along the center line of the metasurface. Most resonators located at $y = 9\,\mathrm{m}$ have the minimum mass of 1 kg, indicating that it is less effective to place resonators here. The resonance frequency of the relevant resonators (with high mass) is between 30 Hz and 85 Hz. In general, resonators with higher resonance frequencies are closer to the source.

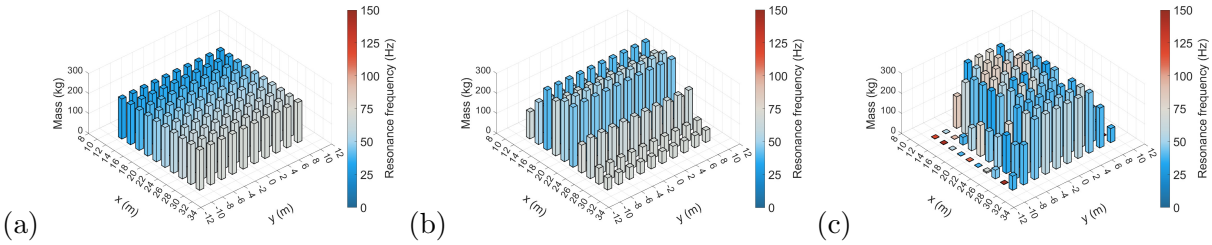

Figure 3: Resonance frequency and mass of the resonators of the (a) inverse metawedge, (b) case 1 and (c) case 2.

The real part of the vertical displacement at 35 Hz, 50 Hz and 65 Hz is shown for a part of the soil domain in figure 4 for all three cases. The resonators are shown with black squares on the soil's surface. Due to the symmetry of the problem, the wave field is symmetric with respect to the xz-plane. Figure 5 shows the corresponding insertion loss, which is defined as:

$$\widehat{\mathrm{IL}}_{zz}(\mathbf{x},\omega) = 20\log_{10}\left|\frac{\hat{u}^{\mathrm{ref}}_{zz}(\mathbf{x},\omega)}{\hat{u}_{zz}(\mathbf{x},\omega)}\right|, \tag{8}$$

where $\hat{u}_{zz}^{\text{ref}}(\mathbf{x},\omega)$ and $\hat{u}_{zz}(\mathbf{x},\omega)$ are the response without and with resonators.

For the inverse metawedge, vibration reduction is attributed to the convergence of surface waves to body waves when the wavefront reaches the resonators with a resonance frequency close to the excitation frequency [7] (figures 4a,4d and 4h). Figures 5a, 5d and 5h clearly show how the vibration reduction near the soil's surface occurs at the expense of amplification at larger depths due to the conversion of surface to body waves. Vibration reduction is more pronounced at 50 Hz.

Case 1 shows higher vibration reduction at 60 Hz (figures 4i and 5i). In case 2, vibration reduction is slightly higher at 35 Hz (figures 4c and 5c). Moreover, at 50 Hz, a more uniform reduction on the surface of the soil is observed (figures 4f and 5f).

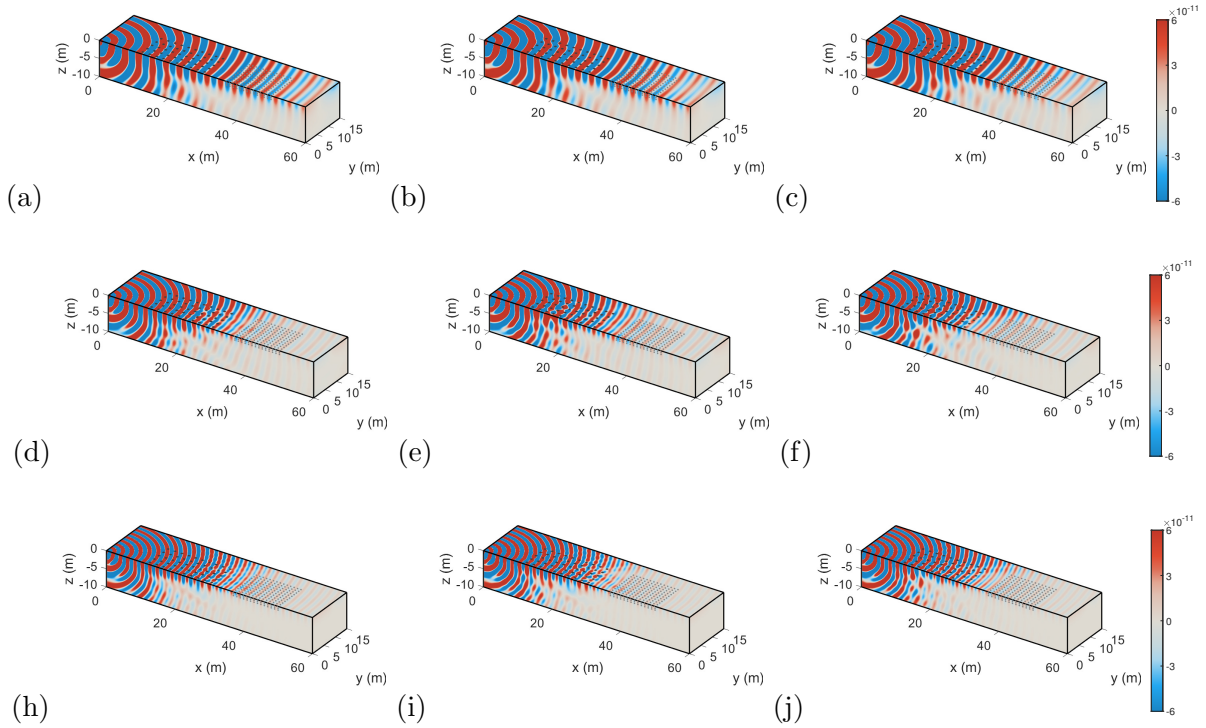

Figure 4: Real part of the vertical displacement $\text{Re}\,(\hat{u}_{zz}(\mathbf{x},\omega))$ [m/Hz] at (a-c) 35 Hz, (d-f) 50 Hz, and (h-j) 65 Hz for (a,d,h) the inverse metawedge,(b,e,i) case 1 and (c,f,j) case 2.

The performance of all cases is now evaluated by considering the vertical mobility of a grid of receivers in a volume Ω_{obs} with center at $x = 44$ m and dimensions and 12 m $\times$ 20 m $\times$ 1 m as shown in figure 6. The position of each receiver is shown with a black point in figures 4 and 5. As a global measure of the response over the grid Ω_{obs} the spatially averaged mobility is superimposed in figure 6. Although the resonance frequencies of the resonators in the inverse metawedge are graded between 30 Hz and 70 Hz, the averaged vertical mobility shows a reduction between 25 Hz and 55 Hz and the performance drops for higher frequencies (figure 6a). This is due to the fact that interaction of the resonators with the soil results in a reduction of the previously mentioned resonance frequencies for resonators on a fixed base. Case 1 enhances the

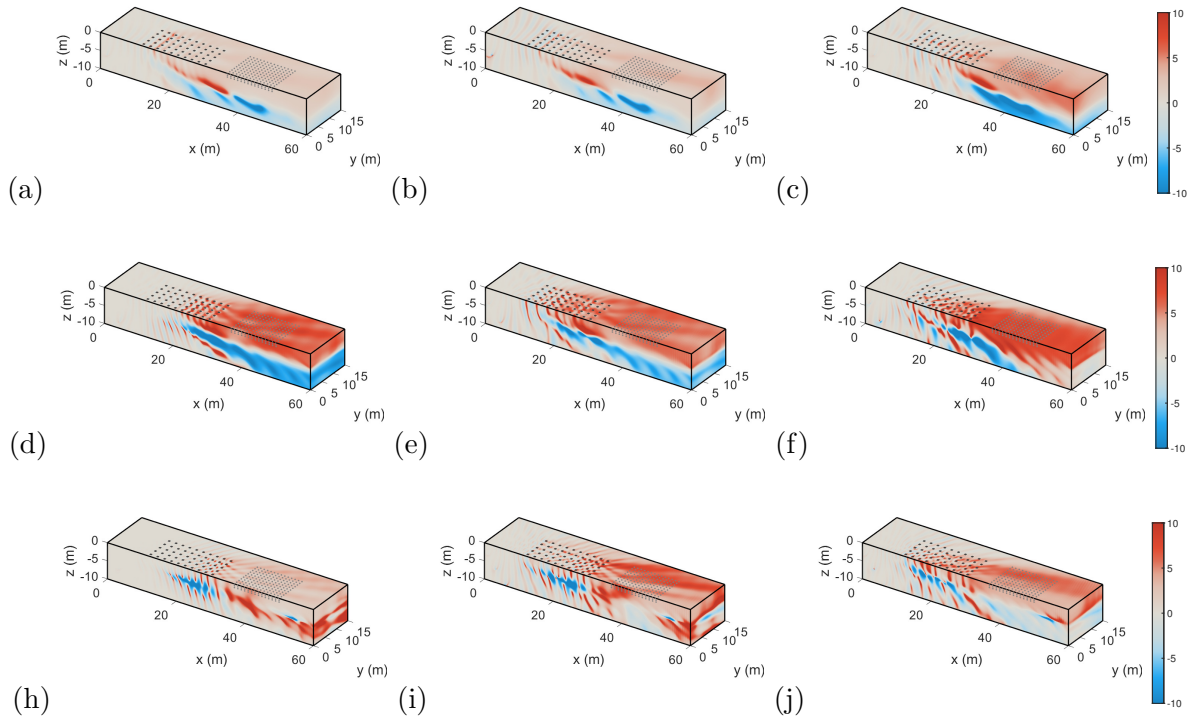

Figure 5: Vertical insertion loss $\widehat{\mathrm{IL}}_{zz}(\mathbf{x},\omega)$ [dB] at (a-c) 35 Hz, (d-f) 50 Hz, and (h-j) 65 Hz for (a,d,h) the inverse metawedge, (b,e,i) case 1 and (c,f,j) case 2.

vibration reduction in a wider frequency range between 30 Hz and 80 Hz. Case 2 also shows a stronger vibration reduction in a wider frequency range. Moreover, the reduction in vertical mobility of each receiver is highly similar, indicating a more uniform vibration reduction.

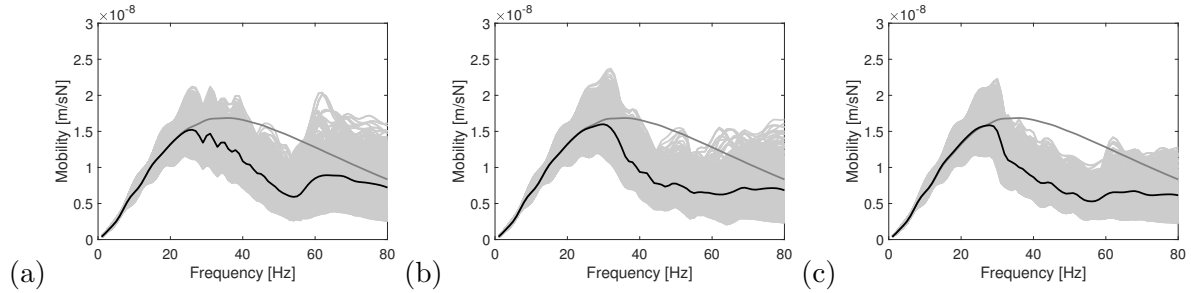

Figure 6: Modulus of the vertical mobility of all receivers in Ω_{obs} for the (a) inverse metawedge, (b) case 1 and (c) case 2. Superimposed is the averaged mobility with (black) and without (dark gray) metasurface.

In order to compare the vibration reduction performance of the three arrangements, 7a shows

the averaged insertion loss over the domain Ω_{obs}:

$$\widehat{\overline{\text{IL}}}_{zz}(\omega) = 20\log_{10}\left(\frac{1}{\Omega_{\text{obs}}}\int_{\Omega}\left|\frac{\hat{u}^{\text{ref}}_{zz}(\mathbf{x},\omega)}{\hat{u}_{zz}(\mathbf{x},\omega)}\right|\,\text{d}\Omega\right). \tag{9}$$

Figure 7b shows the corresponding power flow insertion loss $\langle\widehat{\text{PFIL}}(\omega)\rangle$ through the plane Σ_{p}:

$$\langle\widehat{\text{PFIL}}(\omega)\rangle = 20\log_{10}\left(\frac{\langle\hat{P}^{\text{ref}}_{\text{p}}(\Sigma_{\text{p}},\omega)\rangle}{\langle\hat{P}_{\text{p}}(\Sigma_{\text{p}},\omega)\rangle}\right). \tag{10}$$

The results in figure 7b are consistent with those in figure 7a, demonstrating that optimization enhances vibration reduction in a wider frequency range when compared to the inverse metawedge. The results also confirm that power flow is an effective global measure of vibration reduction as the global trends in figures7a and 7b are similar.

.

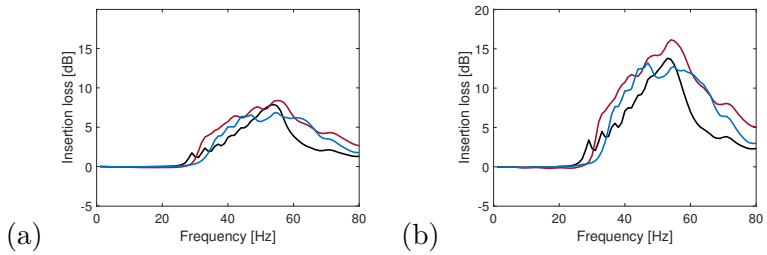

Figure 7: (a) averaged vertical insertion loss for all receivers in Ω_{obs} and (b) power flow insertion loss through the plane Σ_{p} for the inverse metawedge (black), case 1 (blue) and case 2 (red).

5 Conclusion

The performance of seismic metasurfaces in broadband vibration mitigation is optimized based on power flow analysis. We evaluate the efficiency of the metasurfaces by calculating the power flow through a plane behind the metasurface in the soil. The mass and the resonance frequency of the resonators are design variables. Two cases are considered. In case 1, the dynamic parameters of each row of the resonators are design variables. In case 2, a more complex configuration is considered where the dynamic parameters of each resonator are optimized individually. The optimization problem relies on a 3D coupled finite element-boundary element method where the resonators are modeled as single-degree-of-freedom systems on top of square concrete foundations placed on top of layered soil. The optimized configurations are compared to an inverse metawedge. Both optimized solutions enhance the vibration reduction in a wider frequency range. Making the design more complicated is not found to significantly improve the performance. The results show that optimization can be a powerful tool to tune the properties of the metasurface to the specific characteristics and needs of the problem at hand.

Acknowledgment

The results presented in this paper were obtained within the frame of the project G0B8221N "Mitigation of railway induced vibration using seismic metamaterials" funded by the Research

Foundation Flanders (FWO). The financial support is gratefully acknowledged.

REFERENCES

[1] D.P. Connolly, G.P. Marecki, G. Kouroussis, I. Thalassinakis, and P.K. Woodward. The growth of railway ground vibration problems - a review. *Science of the Total Environment*, 568:1276–1282, 2016.

[2] P. Coulier, S. François, G. Degrande, and G. Lombaert. Subgrade stiffening next to the track as a wave impeding barrier for railway induced vibrations. *Soil Dynamics and Earthquake Engineering*, 48:119–131, 2013.

[3] D.J. Thompson, J. Jiang, M.G.R. Toward, M.F.M. Hussein, E. Ntotsios, A. Dijckmans, P. Coulier, G. Lombaert, and G. Degrande. Reducing railway–induced ground–borne vibration by using open trenches and soft–filled barriers. *Soil Dynamics and Earthquake Engineering*, 88:45–59, 2016.

[4] A. Dijckmans, P. Coulier, J. Jiang, M.G.R. Toward, D.J. Thompson, G. Degrande, and G. Lombaert. Mitigation of railway induced ground vibration by heavy masses next to the track. *Soil Dynamics and Earthquake Engineering*, 75:158–170, 2015.

[5] D. Mu, H. Shu, L. Zhao, and S An. A review of research on seismic metamaterials. *Advanced Engineering Materials*, 22(4):1901148, 2020.

[6] K. Zhang, J. Luo, F. Hong, and Z. Deng. Seismic metamaterials with cross-like and square steel sections for low-frequency wide band gaps. *Engineering Structures*, 232:111870, 2021.

[7] A. Colombi, P. Roux, S. Guenneau, P. Gueguen, and R.V. Craster. Forests as a natural seismic metamaterial: Rayleigh wave bandgaps induced by local resonances. *Scientific Reports*, 6:19238, 2016.

[8] A. Colombi, D. Colquitt, P. Roux, S. Guenneau, and R.V. Craster. A seismic metamaterial: The resonant metawedge. *Scientific Reports*, 6:27717, 2016.

[9] P.-R. Wagner, V.K. Dertimanis, E.N. Chatzi, and J.L. Beck. Robust-to-uncertainties optimal design of seismic metamaterials. *ASCE Journal of Engineering Mechanics*, 144(3):04017181, 2018.

[10] D. Carneiro, P. Reumers, G. Lombaert, and G. Degrande. Seismic metasurfaces for broadband vibration mitigation in layered soil. *Soil Dynamics and Earthquake Engineering*, 181(108689):1–15, 2024.

[11] J.T. Xing and W.G. Price. A power–flow analysis based on continuum dynamics. *Philosophical Transactions of the Royal Society A - Mathematical, Physical and Engineering Sciences*, 455:401–436, 1999.

[12] P. Coulier, G. Lombaert, and G. Degrande. The influence of source–receiver interaction on the numerical prediction of railway induced vibrations. *Journal of Sound and Vibration*, 333(12):2520–2538, 2014.

[13] H.G.D. Goyder and R.G. White. Vibrational power flow from machines into built-up structures, part I: Introduction and approximate analyses of beam and plate-like foundations. *Journal of Sound and Vibration*, 68(1):59–75, 1980.

[14] A. Palermo, S. Krödel, A. Marzani, and C. Daraio. Engineered metabarrier as shield from seismic surface waves. *Scientific Reports*, 6:39356, 2016.